A 3D Physics-based Particle Model of the Venus Oxygen Corona: Variations with Solar Activity

V. Tenishev[1], M.R. Combi[1], Y. Shou[1], S. Bougher[1], Y. Ma[2]

[1]Dept. of Climate and Space Sciences and Engineering,University of Michigan
[2]University of California at Los Angeles
[1]2455 Hayward Street,Ann Arbor, MI 48109-2143
[2]Los Angeles, CA 90095

Key Points:

- The density of Venus' extended oxygen corona varies almost by factor a of six of magnitude during a solar cycle.
- Venus' extended oxygen corona was observed by the Pioneer Venus Orbiter (PVO) only at solar maximum conditions.
- Kinetic modeling reproduces PVO observations of Venus' "hot" oxygen corona when forward scattering of the energetic oxygen atoms is employed.
- The strong dependence of the oxygen density in the corona from solar conditions suggested by results of our modeling is consistent with the non-detection of the oxygen corona from Venus Express conducted at solar minimum consitions.

Corresponding author: Valeriy Tenishev, vtenishe@umich.edu

This is the author manuscript accepted for publication and has undergone full peer review but has not been through the copyediting, typesetting, pagination and proofreading process, which may lead to differences between this version and the Version of Record. Please cite this article as doi: 10.1029/2021JA030168.

Abstract

Due to Venus not having a substantial planetary magnetic field the fast-flowing solar wind plasma can propagate to regions close to the planet. Therefore, thermal atomic oxygen in the thermosphere, hot oxygen in the corona, and the resulting pickup oxygen ions are essential for determining the overall interaction of the planet with plasma of the ambient solar wind. To investigate this complex system, we have initiated a project where a combination of Venus Thermosphere General Circulation Model (VTGCM) and Adaptive Mesh Particle Simulator (AMPS) codes are used to determine the variability of the "hot" O corona depending on the solar conditions.

Here we present the results of modeling Venus' oxygen corona using the VTGCM ionosphere/thermosphere and AMPS kinetic particle models. VTGCM produces a self-consistent calculation of the thermosphere/ionosphere, providing the spatial distributions of the dominant species. That is further used in AMPS' modeling of Venus' exosphere (1) to specify the source of the newly created hot O atoms produced by dissociative recombination of O_2^+ ions and (2) to account for thermalization of these energetic oxygen atoms as they propagate in the upper thermosphere.

The altitude distribution of hot O calculated for the solar maximum conditions agree well with Pioneer Venus Orbiter observations of the oxygen corona. The modeling that we have performed for the solar minimum conditions indicates a decrease of the oxygen density in the corona by almost a factor of six compared to that at solar maximum. That is consistent with the non-detection of the oxygen corona from Venus Express. As expected, the solar moderate case is between the solar maximum and minimum cases.

Plain Language Summary

Here we present an investigation of the variability of Venus' extended oxygen corona. For that, we employ a combination of fluid modeling for simulating Venus' ionosphere and thermosphere and kinetic modeling of the source and transport of energetic hot O atoms in the thermosphere. We have found a good agreement of the model results with the Pioneer Venus Orbiter observations of the "hot" O corona. We also found that the oxygen density strongly depends on solar conditions and varies by a factor of six over a solar cycle. That explains why the extended oxygen corona was observed only at the solar maximum. The result presented in this paper will be a part of a later study of the planet's interaction with the ambient solar wind, where the corona model would be used to calculate the mass loading coefficient.

1 Introduction

Venus' extended oxygen corona is in non-equilibrium conditions. Hence, quantitative characterization of the "hot" O population in the corona can only be done based on kinetic modeling. We have employed this approach in the work presented in this paper. One of the first attempts to apply kinetic simulations to study Venus' corona was made by Nagy et al. (1981), who had produced 1D models for the hot atomic coronae based on a two-stream calculation and Liouville's equation. Hodges and Tinsley (1986) generated a Monte Carlo particle trajectory model for the hot H corona of Venus, a method that developed finally into 3D Monte Carlo trajectory models for O and C in Venus and Mars (Hodges, 2000). An example of recent kinetic modeling efforts can be found in, e.g., Gröller et al. (2012).

Here we present the first results of a 3D hot O corona calculation and its variation with solar activity based on the detailed physics and chemistry of the thermosphere and ionosphere. The presented modeling is performed using a combination of a fluid-type Venus' ionosphere/thermosphere model (VTGCM) and kinetic model AMPS. In this study, we

have used AMPS to simulate the source and transport of the energetic hot O accounting for their thermalization in the thermosphere. The paper presents both the model results and comparison with PVO observations of Venus' hot O corona.

Kinetic modeling of Venus exosphere and corona presented in this paper is based on our previous modeling work of Mars' extended oxygen corona. Despite the much lower surface pressure and two times larger heliocentric distance for Mars than Venus, CO_2 dominates their lower atmospheres, and both planets have surprisingly similar thermospheres and ionospheres. In addition, they both lack a dominant global dipole magnetic field in shaping the interaction of the solar wind with the planet. As such, the production mechanism of the two exospheres is also similar. Because of its larger mass, Venus' corona does not contribute to substantial mass loss, while escape of Mars' hot O corona is thought to be the biggest contributor to mass loss (Y. Lee, Combi, Tenishev, Bougher, & Lillis, 2015; Valeille, Tenishev, et al., 2009; Valeille, Combi, et al., 2009; Fox & Hac, 2009; Lillis et al., 2015; Cravens et al., 2017).

In future work, this hot O corona and the self-consistent thermal O distribution of the thermosphere/ionosphere model will be used to investigate the interaction of the solar wind with Venus.

2 Venus' upper atmosphere and corona

Venus' exosphere, thermosphere and ionosphere have been studied based on spacecraft observations for many years, since the Soviet Venera and US Mariner eras, during the nearly 14-year Pioneer Venus mission, and up to the present time with the Venus Express mission (S. W. Bougher et al., 1997; Schubert et al., 2007; Gérard et al., 2017).

Most of our current knowledge of Venus' upper atmosphere and corona comes from measurements made by in-situ and remote sensing experiments on the Pioneer Venus Orbiter (PVO) from December 1978 to October 1992. The "hot" O corona was observed with an ultraviolet spectrometer (UVS) onboard PVO by measuring the OI resonance triplet near 1304 Å(Nagy et al., 1981). Based on these observations Nagy et al. (1981) had derived the density of "hot" O population on the order of 10^4 cm^{-3} at the altitude range $400 - 800$ km.

PVO had also performed observations of Venus' ionosphere. Mainly, the data relevant to Venus' ionosphere was obtained with the orbiter radio occultation experiment (ORO), the Ion Mass Spectrometer (OIMS), the Retarding Potential Analyzer (ORPA), and the Langmuir Probe (OETP) (e.g., Brace et al., 1980; Taylor et al., 1980; Knudsen et al., 1980). Most recently, the VEx Radio Science (VeRA) experiment returned many electron density profiles using the radio occultation technique (e.g., Pätzold et al., 2007).

The "hot" O density estimation derived from the PVO/UVS data was not confirmed by later observations. SPICAV and ASPERA-4 onboard Venus Express had sufficient sensitivity to detect the "hot" O population if the density of this population is of the order that was derived from the PVO data (Bertaux et al., 2007; Galli et al., 2008). However, "hot" oxygen was not detected above the instrument threshold neither by SPICAV or ASPERA-4 (Lichtenegger et al., 2009).

This 'first-order' picture of Venus' upper atmosphere winds has been gleaned from a number of remote and in-situ datasets collected at the planet. A thorough examination of Pioneer Venus Orbiter (PVO) neutral density (e.g., CO_2, O, He, and H) and temperature distributions above $\sim$130 km, as well as ultraviolet (UV) NO nightglow and O dayglow distributions, has been used to constrain general circulation model simulations, from which SS-AS and RSZ wind magnitudes can be extracted (see reviews by S. Bougher et al. (2006)). In addition, visible and infrared O_2 nightglow distributions from Venera 9 and 10, Galileo, PVO, and the ground, along with minor species distributions (espe-

cially CO) have also been used to constrain upper mesospheric wind patterns (80-110 km) (e.g., Schubert et al., 2007; Lellouch et al., 1998).

Systematic monitoring by VEx instruments (since 2006) augments this record with measurements of key nightglow distributions (e.g., NO, O_2) and vertical structure measurements needed to infer SS-AS and RSZ wind variations and any residuals (A. Brecht et al., 2011). For example, Visible and IR Thermal Imaging Spectrometer (VIRTIS) observations address upper atmosphere dynamics by (1) measuring the 3-D temperatures and deriving the thermal wind fields ($\sim 40-90$ km) (Piccialli et al., 2008, 2012), and (2) mapping the highly variable O_2 IR nightglow distribution (e.g., Drossart et al., 2007; Gérard, Saglam, et al., 2008, 2009; Hueso et al., 2008; Piccioni et al., 2009; Soret et al., 2012, 2014) as a tracer of the wind system over $\sim$90 to 130 km. Also, Spectroscopy for Investigation of Characteristics of the Atmosphere of Venus (SPICAV) airglow (nadir and limb) observations of NO (190-270 nm) emissions were made and modeled (Gérard, Cox, et al., 2008, 2009; Collet et al., 2010; Stiepen et al., 2013). Nadir viewing enables NO nightglow maps to be constructed (Stiepen et al., 2013), confirming the pattern observed previously with PVO (Stewart et al., 1980). Furthermore, SPICAV provides repeated measurements of vertical profiles of atmospheric density (and inferred temperatures) over $\sim 80-150$ km (nightside) via stellar occultations (e.g., Bertaux et al., 2007). These VEx datasets have been used to validate VTGCM simulations (A. Brecht et al., 2011, 2012; A. Brecht & Bougher, 2012; S. Bougher et al., 2015). In summary, departures from this basic 2-component wind model (residuals) are becoming more apparent as ground-based and multiple VEx observations are combined with previous PVO measurements.

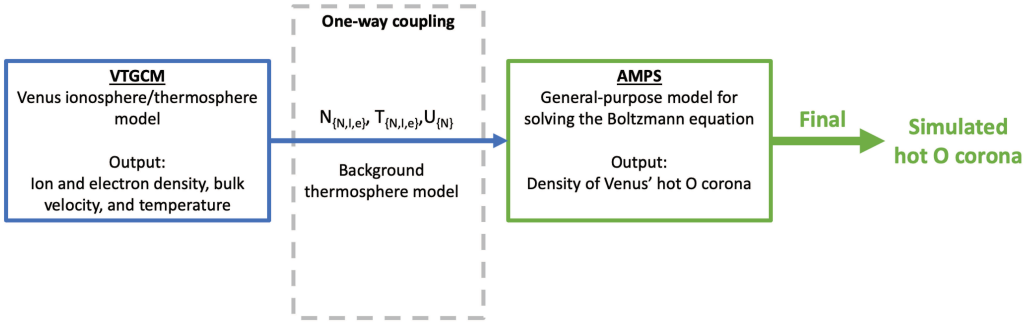

Figure 1. The figure illustrates the implemented coupling approach. First, we use VTGCM to simulate Venus' ionosphere and thermosphere. Then, the calculated (1) density, bulk velocity, and temperatures of the primary neutral species and (2) density of ions and electrons are passed to AMPS for modeling the extended hot oxygen corona, which is the final result of the study presented here.

3 Consistent Thermosphere/Ionosphere/Exosphere Model

Here we describe the current state of the core modeling tools that we have used in this paper. The order of presenting the models repeats the order that the models are used in the actual simulations, as illustrated in Fig. 1. Hence, we start with the Venus Thermosphere General Circulation model (VTGCM) continuing with the Adaptive Mesh Particle Simulator (AMPS).

3.1 Venus Thermosphere General Circulation model (VTGCM)

The Venus Thermosphere General Circulation Model (VTGCM) is a 3-D finite difference hydrodynamic model of Venus' upper atmosphere (S. Bougher et al., 1988) which is based on the National Center for Atmospheric Research terrestrial Thermospheric General Circulation Model (TGCM). The VTGCM has been well documented in the literature as it has been revised and improved over the last three decades. This section presents an overview of the model as implemented recently and used to interpret Venus Express datasets (e.g., A. Brecht et al., 2011, 2012; A. Brecht & Bougher, 2012; S. Bougher et al., 2015).

The VTGCM solves the time-dependent Navier Stokes equations for the neutral upper atmosphere. The diagnostic equations (hydrostatic and continuity) are solved to provide geopotential and vertical motion fields. The prognostic equations (thermodynamic, eastward and northward momentum, composition) are solved for steady-state solutions for the temperature, zonal and meridional velocity, and the mass mixing ratios of specific species (e.g., O, CO, N_2, CO_2, O_2, OH, N, NO, SO, SO_2). The VTGCM model domain covers a $5^\circ \times 5^\circ$ latitude-longitude grid, with 1/2-scale height evenly spaced log-pressure levels (69) in the vertical, extending from $\sim$ 70 to 300 km ($\sim$ 70 to 200 km) at local noon (midnight). This altitude range captures the key dynamical processes contributing to the nightglow layers (i.e. NO, O_2, OH), and ensures that wave propagation above the cloud tops can be addressed. The lower boundary of the VTGCM has recently been modified to include the self-consistent latitude and local time variation of temperatures, zonal and meridional winds, plus heights near $\sim$69 km. This specification is in accord with current Venus lower atmosphere General Circulation Models (e.g., C. Lee & Richardson, 2010).

The VTGCM ionosphere is calculated from direct photo-ionization of CO_2 and O, producing CO_2^+ and O^+ initially. The reaction of CO_2^+ with O produces O_2^+, directly. Alternatively, the reaction of O^+ with CO_2 ultimately (2-step) produces O_2^+ as well. These photochemical reactions enable O_2^+ to be produced and subsequently to dissociatively recombine, yielding the hot O atoms discussed in Section 3.2. This photochemical treatment is adequate to calculate the bulk of the hot O production (below 200 km) on the dayside. Nightside production of hot O is minimal by comparison and is neglected.

The VTGCM includes fast parameterizations for CO_2 15$-\mu$m cooling, infrared (IR) heating, and extreme ultraviolet (EUV) heating. The near-IR heating rate is incorporated in the VTGCM using two offline simulated look-up tables (organized as a function of pressure and SZA), and taken from Roldán et al. (2000) and Crisp (1986) for the upper and middle atmosphere, respectively. Reference CO_2 15$-\mu$m cooling rates for a given temperature and composition profile are taken from Roldán et al. (2000). Subsequently, local cooling rates are simulated for VTGCM temperatures and species abundances from these reference rates (S. Bougher et al., 1986). In addition, the VTGCM can capture the full range of EUV-UV flux conditions, yielding neutral heating, photodissociation and ionization rates. The corresponding ion-neutral reactions and rates being used in the VTGCM are primarily taken from Fox and Sung (2001).

Since sub-grid scale wave effects cannot be captured by the VTGCM directly, empirically based parameterizations are applied instead. For instance, wave drag is presently prescribed as Rayleigh friction within the VTGCM in order to mimic first order wave-drag effects on the mean flow (e.g., A. Brecht et al., 2011). However, detailed gravity wave momentum and energy deposition schemes are being tested for replacement of Rayleigh friction within the VTGCM code (Zalucha et al., 2013). In addition, the eddy diffusion coefficient is prescribed within the VTGCM using a standard aeronomical formulation and constrained using Pioneer Venus measurements (e.g., von Zahn et al., 1979; A. Brecht et al., 2011).

Historically, statistically averaged maps of nightglow emission distributions from Venus measurements during both Pioneer Venus and Venus Express (VEx) missions have provided constraints for the mean thermospheric circulation of the Venus upper atmosphere (e.g., S. Bougher et al., 2006). Specifically, 2-D maps of O_2, NO, and OH nightglow emission distributions have been constructed and compared to climate maps of VTGCM simulated nightglow distributions (e.g., A. Brecht et al., 2011; Parkinson et al., 2021). These comparisons have been used to study the time averaged behavior of both the sub-solar to anti-solar (SS-AS) and the super-rotating retrograde zonal (RSZ) components of the atmospheric circulation above the cloud tops. In addition, the Venus Express mission has prompted the study of VTGCM climate model outputs of terminator temperature profiles for comparison with corresponding statistically averaged SOIR profiles in 5-latitude bins (S. Bougher et al., 2015).

However, it is noteworthy that the VTGCM thus far has largely been used as a climate model. Nevertheless, the changing SS-AS and RSZ wind components of the real atmosphere provide significant variations of these densities, temperatures, and nightglow distributions over time. Additional tidal wave, planetary wave, and gravity wave formulations are presently being incorporated into the VTGCM framework to test the impacts of these waves (of various scales) on the time varying upper atmosphere circulation, corresponding density and temperature structure, and changing nightglow distributions (A. S. Brecht et al., 2021).

3.2 Adaptive Mesh Particle Simulator (AMPS)

Important processes in tenuous atmospheres work on various energy and rate scales described with the Boltzmann equation. AMPS is a general-purpose multi-species kinetic code for solving the Boltzmann equation using the Direct Simulation Monte Carlo (DSMC) method (Bird, 1994). Nowadays, DSMC is the de facto standard method in the broad rarefied gas community to provide useful solutions to the generalized collisional Boltzmann equation (Combi et al., 2004). The details of the code capabilities and implemented physics models are given in our recent paper by Tenishev et al. (2021, 2013).

DSMC was first used to simulate the transition regime, where the mean free path of particles is too large for continuum hydrodynamics to be applicable. Simulation particles move around within a grid, colliding with other particles and any solid objects. Macroscopic properties (density, velocity and temperatures) are computed by appropriately averaging particle masses, locations, velocities, and internal energies. DSMC is based on the 'rarefied-gas' assumption that over a short time interval or 'step' the molecular motion and the intermolecular collisions are uncoupled and can be calculated independently. Molecules move over the distances appropriate for this time step, affected by macroscopic forces (e.g., gravity, radiation pressure, or Lorentz force for charged particles) as necessary, followed by calculating a representative set of collisions. The time step needs to be smaller compared to the mean collision time.

For this work, we adapted Mars' oxygen corona application developed in AMPS that used in our previous studies for the case of Venus' environment. That is possible because both Mars and Venus have similar mechanisms for producing and thermalizing energetic hot O. These previous Mars modeling are described in a series of papers by e.g., Valeille, Tenishev, et al. (2009), Valeille, Combi, et al. (2009), and Y. Lee, Combi, Tenishev, Bougher, Deighan, et al. (2015).

The parameters of the dissociative recombination reaction that was employed in this study are summarized in Table 1. The reaction rate constant in Eq. 1 was adapted from Mehr and Biondi (1969), which was also used in our previous investigation of Mars' hot O corona (e.g., Y. Lee, Combi, Tenishev, Bougher, & Lillis, 2015; Valeille et al., 2010).

$$O_2^+ + e \rightarrow \begin{cases} \text{Reaction channel} & \text{Excess energy} & \text{Branching ratio} \\ \hline O(3P) + O(3P) & 6.98\ \text{eV} & 0.22 \\ O(3P) + O(1D) & 5.02\ \text{eV} & 0.42 \\ O(1D) + O(1D) & 3.05\ \text{eV} & 0.31 \\ O(1D) + O(1S) & 0.83\ \text{eV} & 0.05 \end{cases}$$

Table 1. O_2^+ dissociative recombination channels, excess energies, and branching rations. Adapted from Kella et al. (1997).

$$\alpha = \begin{cases} 1.95 \times 10^{-7} \left(\frac{300}{T_e}\right)^{0.7} \text{cm}^3\text{s}^{-1}, & 300 < T_e < 1200\text{K} \\ 7.39 \times 10^{-8} \left(\frac{1200}{Te}\right)^{0.56} \text{cm}^3\text{s}^{-1}, & 1200 < T_e < 5000\text{K} \end{cases} \quad (1)$$

Propagating in the thermosphere, the energetic hot O may experience collisions with atoms and molecules populating the ambient thermosphere, lose their energy and become thermalized before reaching the corona. Overlapping VTGCM and AMPS model simulations are conducted (130 to 200 km). Extrapolation of CO_2, O, N_2, CO to higher altitudes by the exponential method is used.

The thermospheric wind has no significant direct effect on the "hot" O distribution. Among all simulated channels of O_2^+ dissociative recombinations, the smallest excess energy is 0.83 eV, which corresponds to a velocity of the newly created oxygen atoms of 9 km/s. Thermospheric wind does not exceed 200 m/s, which is much smaller than the velocity of energetic oxygen atoms. Therefore, collisions of the energetic oxygen atoms are mainly determined by their speed, not thermospheric winds. In our modeling, the newly created energetic oxygen atoms are created in the frame of reference that moves with the O_2^+ bulk flow, which also accounts for the potential wind's effect. However, the wind can affect the final dayside O_2^+ distribution that is a source of the energetic oxygen atoms.

Collisions of a hot energetic O with a thermal O from the ambient thermosphere can energize the latter sufficiently to reach the corona. This process is also accounted for in AMPS' simulations. The energy that is transferred during collisions is highly dependent on both the total and angular differential scattering cross-sections. In work presented here, we have used the forward scattering cross-sections by Kharchenko et al. (2000). We also have used these cross-sections in our studies of Mars' oxygen corona (e.g., Y. Lee et al., 2018, 2020). The effect of producing secondary hot O is discussed by, e.g., Y. Lee, Combi, Tenishev, Bougher, and Lillis (2015).

4 Results

This section summarizes results of the study that we have presented here. The distinctive feature of the presented modeling is that it combines modeling of Venus' ionosphere/thermosphere with kinetic modeling of the corona. Section 4.1 summarize the VTGCM simulations that were used as input for further modeling the hot oxygen corona. The detailed discussion of the variability of the corona that we have inferred from our modeling is in section 4.2.

4.1 Thermosphere and ionosphere input for solar maximum, moderate, and minimum conditions

The VTGCM can capture the full range of EUV-UV flux conditions (see section 3.1). For this paper, solar fluxes were specified, making use of the Solomon flux bins and

solar fluxes based upon the Hinteregger linear interpolation method, which makes use of the F10.7-cm index at Earth (e.g., Hinteregger et al., 1981; S. W. Bougher et al., 2002; A. S. Brecht et al., 2021). These fluxes (0.1 to 225.0-nm) are scaled to the Venus-sun distance by multiplying by a factor of 1.914. Three F10.7-cm solar flux periods are chosen for VTGCM simulations presented in this paper: (a) solar minimum (early Venus Express sampling) conditions, for which F10.7 = 70; (b) solar moderate (Magellan sampling) conditions, where F10.7 = 130; and (c) solar maximum (early Pioneer Venus sampling) conditions, for which F10.7 = 170 or 200. These calculations are illustrated in Figs. 2, 3, and 4.

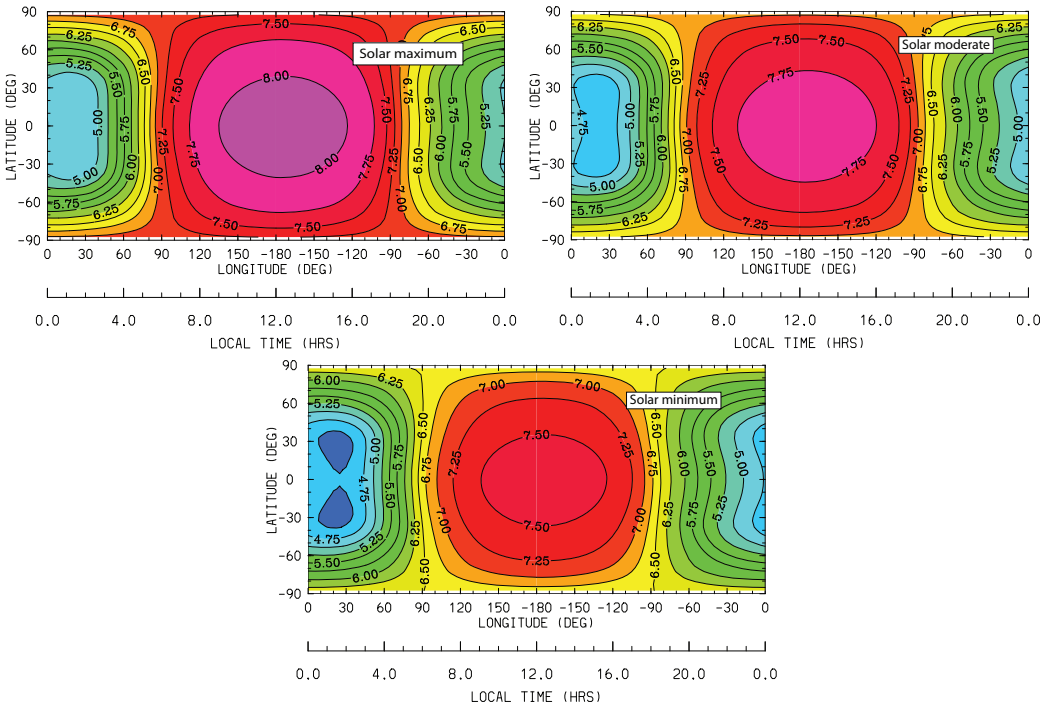

Figure 2. Thermal neutral oxygen distribution at a 200 km exobase for solar maximum, moderate, and minimum cases. The contour values are in base ten log of the density in cm^{-3}.

4.2 Structure and Solar Activity Variation of the Hot O Corona

We have calculated the content of Venus' hot oxygen corona for solar maximum, moderate, and minimum conditions. The ionosphere and thermosphere have been simulated with the VTGCM model as described in Section 4.1. The results of that modeling was used in the study of hot O corona presented in the paper. The rate of injection of the newly created energetic hot O and their velocity have been determined as summarized in Eq. 1 and Table 1. The interaction of hot O atoms with the background thermosphere was simulated using the forward scattering cross-section by Kharchenko et al. (2000). In the presented simulations, we also account for the secondary production of hot O atoms in collisions of existing hot O atoms with the background thermosphere. Gröller et al. (2012) showed that O_2^+, and thus the production of "hot" O, peaks at 150 km or so, whereas the CO_2 density is only dominant below about 140 km. Hence, the interaction of "hot" O with the CO_2 population would not significantly contribute to the overall interaction of "hot" O with the thermosphere and thus will not result in a significant change of "hot" O densities.

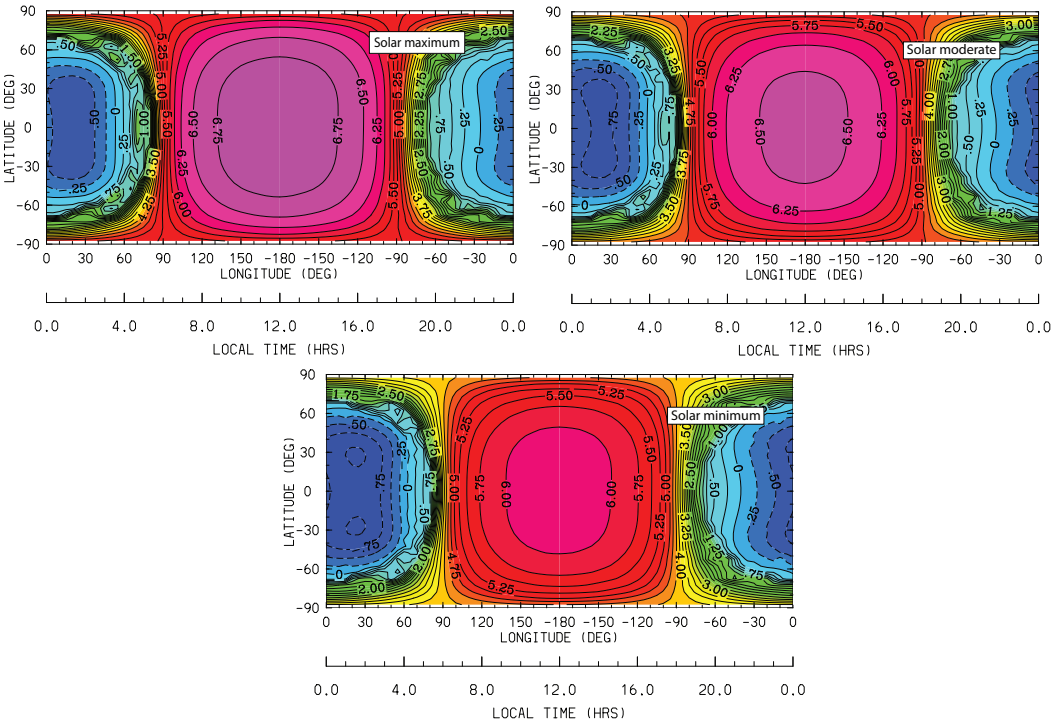

Figure 3. Neutral CO_2 distribution at a 200 km exobase for solar maximum, moderate and minimum cases. The contour values are in base ten log of the density in cm^{-3}.

A model particle was considered thermalized and removed from the simulation if, after a collision, the following criterion is met

$$v_p < 2v_{th}, \tag{2}$$

where v_p is the particle velocity after a collision, and v_{th} is the mean thermal velocity of oxygen atoms at the particle's location.

Fig. 5 shows density of hot oxygen corona in a plane that (1) includes the planet's center and (2) is normal to the ecliptic plane. The presented calculations were performed for solar maximum and minimum conditions to illustrate the range of the corona's variability. Our model results indicate that the hot O population density is mainly axially-symmetric around the sunward direction. One can see that though the overall topology of the corona does not change through the solar cycle, the density has a significant dependence on the solar conditions.

For validation of the model results, we have compared the results of our simulations with the PVO observations of Venus' extended oxygen corona in Fig. 7. The results of our modeling for the appropriate solar maximum conditions are in good agreement with the PVO observations (Gröller et al., 2010). The oxygen density in the corona is significantly affected by the solar conditions, which explains non-detection of the oxygen corona from Venus Express.

Thermal atomic oxygen dominates the overall atomic oxygen population at low altitudes. Density of this thermal population drops with altitude faster than that of the energetic hot atomic oxygen. As a result, at the altitudes above 400 km, the non-thermal hot atomic oxygen dominates the overall oxygen population as presented in Fig. 6.

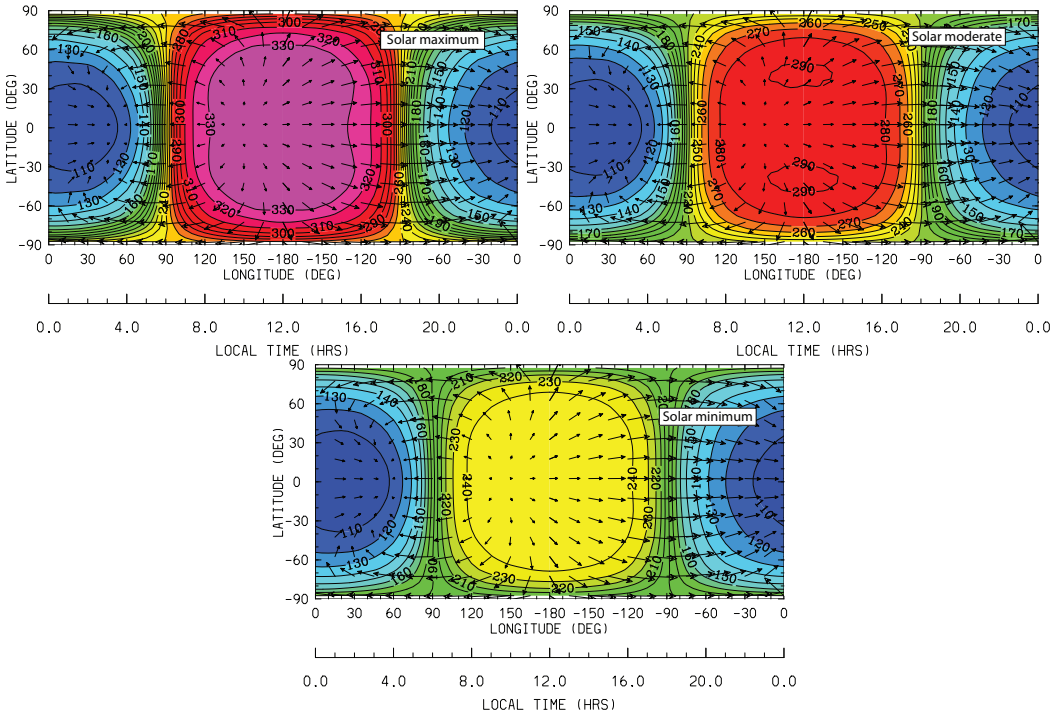

Figure 4. Neutral temperature (K) distribution at a 200 km exobase for solar maximum, moderate and minimum cases. The maximum velocity vectors are as follows:solar maximum (∼335 m/s), moderate (∼305 m/s) and minimum (∼280 m/s), corresponding to the VTGCM cases in these three panels.

5 Summary

This study investigated the variability of Venus' extended hot oxygen corona over a solar cycle and compared the model results with PVO observations of the corona. The modeling was conducted using the Venus' ionosphere/thermosphere model VTGCM and a kinetic model AMPS. Our model results are in good agreement with observations of "hot" O population performed with ultraviolet spectrometer (UVS) onboard PVO that was done by measuring the OI resonance triplet near 1304 Å (e.g., Nagy et al., 1981; Paxton & Meier, 1986). For this study, we have taken the data from Gröller et al. (2010).

We have reproduced the PVO/UVS observations with our kinetic simulation of hot O transport in Venus' thermosphere, exosphere and corona. We also found that accounting for the forward scattering of energetic oxygen atoms when they collide with the thermal thermosphere population is needed. The latter is consistent with conclusions by, e.g., Gröller et al. (2010).

Our modeling suggests that density of the extended oxygen corona varies by a factor of six during a solar cycle. That agrees with Gérard et al. (2017), who suggest that density at low solar activity during the Venus Express era was up to a factor of 5 smaller than that during solar maximum conditions at PVO observations.

Neither ASPERA-4 nor SPICAV onboard Venus Express have confirmed PVO observations (Gérard et al., 2017). The strong dependence of the oxygen density in the corona on the solar conditions suggested by our modeling is consistent with the non-detection of the oxygen corona from Venus Express (Lichtenegger et al., 2009). That makes the solar maximum most favorable for observing the oxygen corona of Venus.

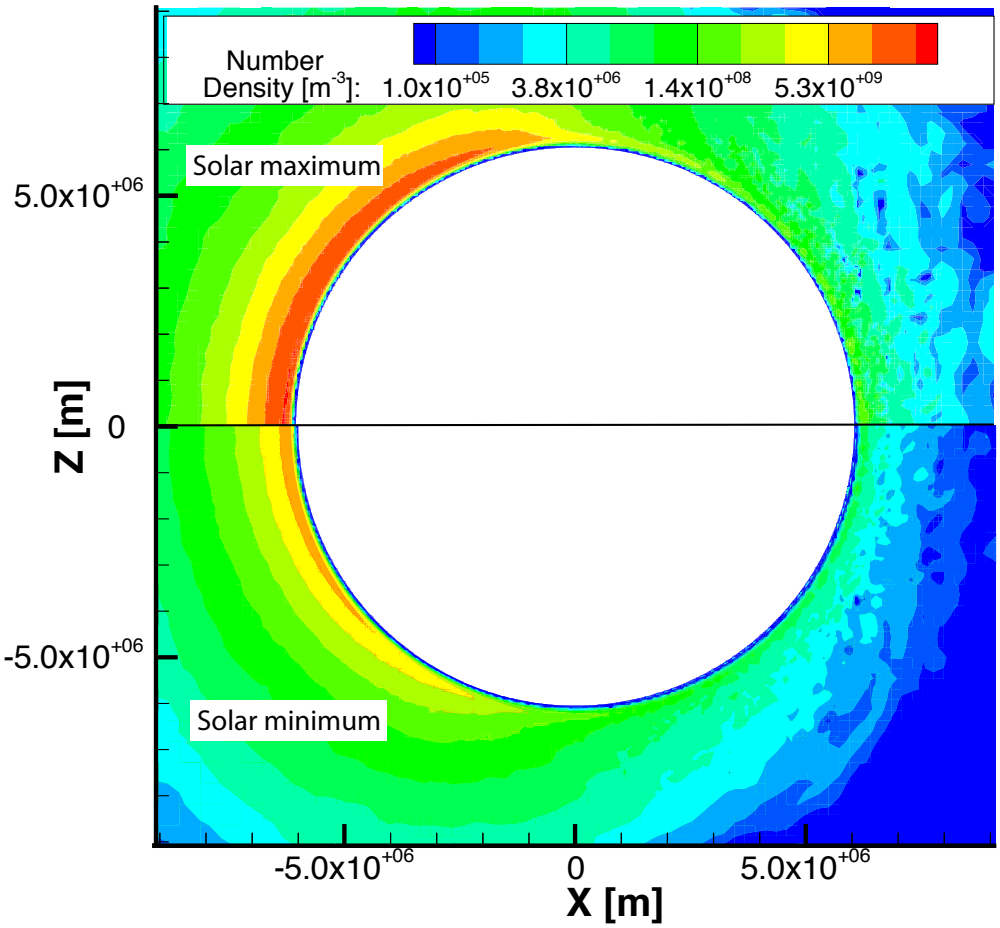

Figure 5. Density of hot oxygen corona. The figure present a cut of the 3D simulation performed for solar maximum and minimum cases. The solar moderate case is intermediate between these two. The axis are defined as follow: X-axis is directed away from the Sun (X-axis points toward the nightside), Y-axis is in the ecliptic plane, normal to X-direction and anti-parallel to the planet's velocity relative to the Sun. Z-axis is a cross product of X- and Y- axis.

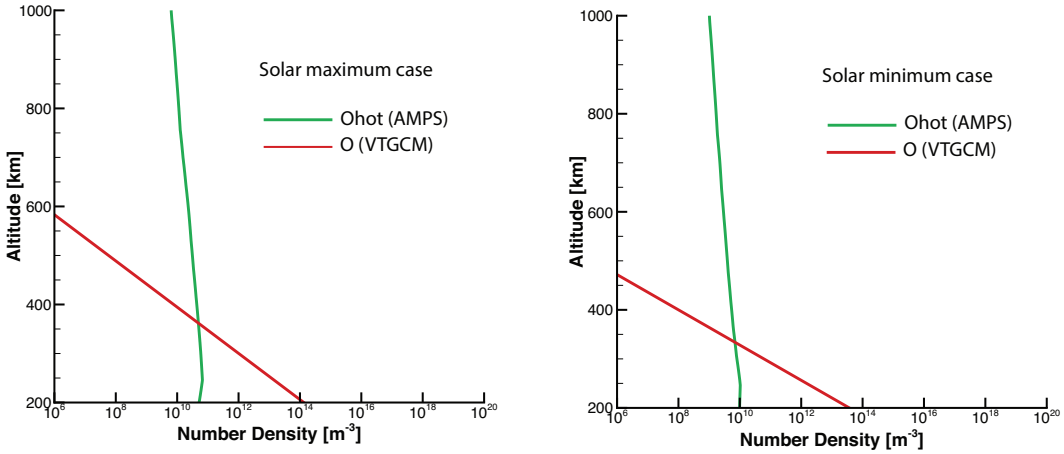

Figure 6. Vertical sub-solar density profiles of oxygen calculated with AMPS model (green) and derived from the VTGCM model (red) for solar maximum and minimum conditions. One can see that at altitudes above 400 km, energetic hot oxygen dominates the total oxygen population both the solar minimum and maximum cases.

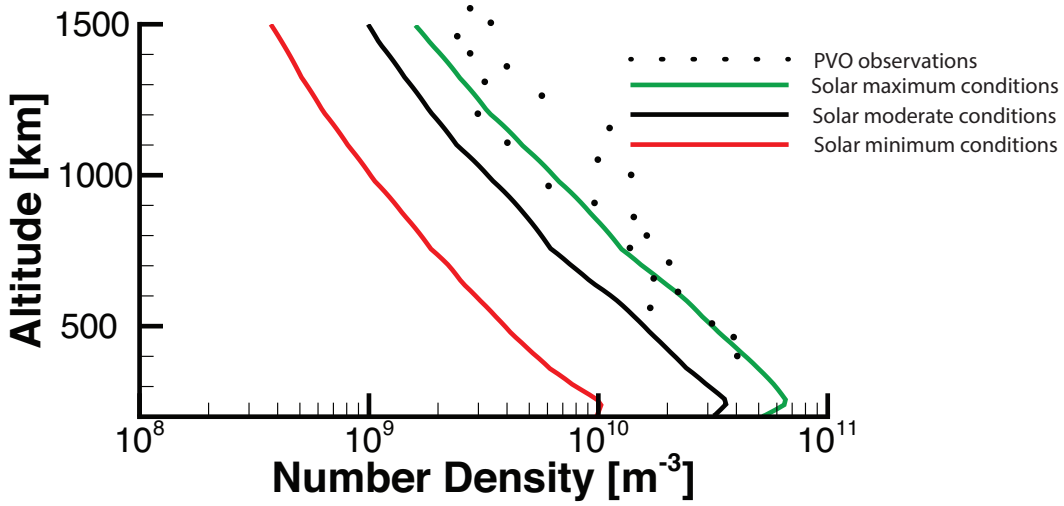

Figure 7. Simulated altitude variation of "hot" oxygen population. The lines show the solar minimum, moderate and maximum model results. The dots are density of "hot" oxygen atoms derived from measurements of the OI resonance triplet near 1304 Å by the ultraviolet spectrometer onboard PVO. The measurements were performed at solar maximum (Nagy et al., 1981; Paxton & Meier, 1986). The data was adapted from Gröller et al. (2010).

6 Data Availability Statement

Data in Figures 2-7 are available in the University of Michigan Deep Blue Data archive (collection https://doi.org/10.7302/x094-he85).

Acknowledgments

Support for this work is provided by NASA grant 80NSSC17K0728 from the Solar System Workings Program. Computer resources were provided by the NASA High End Computing facility at NASA Ames under award HEC-SMD-17-1633.

References

Bertaux, J.-L., Vandaele, A.-C., Korablev, O., Villard, E., Fedorova, A., Fussen, D., ... Rodin, A. (2007). A warm layer in Venus' cryosphere and high-altitude measurements of (hf), (hcl), $(h)_2(o)$ and (hdo). *Nature*, *450*, 646–649.

Bird, G. (1994). *Molecular gas dynamics and the direct simulation of gas flows*. Oxford University Press.

Bougher, S., Brecht, A., Schulte, R., Fischer, J., Parkinson, C., Mahieux, A., ... Vandaele, A. (2015). Upper atmosphere temperature structure at the Venusian terminators: A comparison of SOIR and VTGCM results. *Planetary and Space Science*, *113-114*, 336 - 346.

Bougher, S., Dickinson, R., Ridley, E., & Roble, R. (1988). Venus mesosphere and thermosphere III. three-dimensional general circulation with coupled dynamics and composition. *Icarus*, *73*, 545-573.

Bougher, S., Dickinson, R., Ridley, E., Roble, R., Nagy, A., & Cravens, T. (1986). Venus mesosphere and thermosphere II. global circulation, temperature, and density variations. *Icarus*, *68*, 284-312.

Bougher, S., Rafkin, S., & Drossart, P. (2006). Dynamics of the Venus upper atmosphere: Outstanding problems and new constraints expected from Venus Express. *Planetary and Space Science*, *54*(13), 1371 - 1380.

Bougher, S. W., Alexander, M. J., & Mayr, H. G. (1997). Venus II : Geology, geophysics, atmosphere, and solar wind environment. In S. W. Bougher (Ed.), (p. 259). Hunten, and R.J. Philips. Tucson, AZ : University of Arizona Press.

Bougher, S. W., Roble, R. G., & Fuller-Rowell, T. J. (2002). AGU Monograph : Comparative aeronomy in the solar system. In M. Mendillo, A. F. Nagy, & J. H. Waite (Eds.), (chap. Simulations of the Upper Atmospheres of the Terrestrial Planets). AGU Books.

Brace, L. H., Theis, R. F., Hoegy, W. R., Wolfe, J. H., Mihalov, J. D., Russell, C. T., ... Nagy, A. F. (1980). The dynamic behavior of the Venus ionosphere in response to solar wind interactions. *Journal of Geophysical Research: Space Physics*, *85*(A13), 7663-7678.

Brecht, A., & Bougher, S. (2012). Dayside thermal structure of Venus' upper atmosphere characterized by a global model. *Journal of Geophysical Research*, *117*, E08002.

Brecht, A., Bougher, S., Gerard, J. C., Parkinson, C. D., Rafkin, S., & Foster, B. (2011). Understanding the variability of nightside temperatures, NO UV and O_2 IR nightglow emissions in the Venus upper atmosphere. *Journal of Geophysical Research*, *116*(E08004).

Brecht, A., Bougher, S., Gérard, J.-C., & Soret, L. (2012). Atomic oxygen distributions in the Venus thermosphere: Comparisons between Venus Express observations and global model simulations. *Icarus*, *217*(2), 759 - 766.

Brecht, A. S., Bougher, S. W., Shields, D., & Liu, H.-L. (2021). Planetary-scale wave impacts on the Venusian upper mesosphere and lower thermosphere. *Journal of Geophysical Research*, *126*, e2020JE006587.

Collet, A., Cox, C., & Gérard, J. C. (2010). Two-dimensional time-dependent model of the transport of minor species in the Venus night side upper atmosphere. *Planetary and Space Science*, *58*(14), 1857-1867.

Combi, M. R., Harris, W. M., & Smyth, W. H. (2004). Comets II. In C. Festou, H. U. Keller, & H. A. Weaver (Eds.), (p. 523-552). University of Arizona Press, Tucson.

Cravens, T. E., Rahmati, A., Fox, J. L., Lillis, R., Bougher, S., Luhmann, J., ... Jakosky, B. (2017). Hot oxygen escape from mars: Simple scaling with solar euv irradiance. *Journal of Geophysical Research: Space Physics*, *122*, 1102–1116.

Crisp, D. (1986). Radiative forcing of the Venus mesosphere: I. solar fluxes and heating rates. *Icarus*, *97*(3), 484-514.

Drossart, P., Piccioni, G., Gérard, J. C., Lopez-Valverde, M. A., Sanchez-Lavega, A., ... the VIRTIS-Venus Express Technical Team (2007). A dynamic upper atmosphere of Venus as revealed by VIRTIS on Venus Express. *Nature*, *450*(641-645).

Fox, J. L., & Hac, A. B. (2009). Photochemical escape of oxygen from Mars: A comparison of the exobase approximation to a Monte Carlo method. *Icarus*, *204*, 527–544.

Fox, J. L., & Sung, K. Y. (2001). Solar activity variations of the Venus thermosphere/ionosphere. *Journal of Geophysical Research*, *106*(A10), 21,305-21,335.

Galli, A., Fok, M.-C., Wurz, P., Barabash, S., Grigoriev, A., Futaana, Y., ... Gunell, H. (2008). Tailward flow of energetic neutral atoms observed at venus. *Journal of Geophysical Research*, *113*, E00B15.

Gérard, J.-C., Bougher, S., López-Valverde, M., Pätzold, M., Drossart, P., & Piccioni, G. (2017). Aeronomy of the Venus upper atmosphere. *Space Science Reviews*.

Gérard, J. C., Cox, C., Saglam, A., Bertaux, J., Villard, E., & Nehmé, C. (2008). Limb observations of the ultraviolet nitric oxide nightglow with SPICAV on board Venus Express. *Journal of Geophysical Research*, *113*, E12.

Gérard, J.-C., Cox, C., Soret, L., Saglam, A., Piccioni, G., Bertaux, J.-L., & Drossart, P. (2009). Concurrent observations of the ultraviolet nitric oxide and infrared O_2 nightglow emissions with Venus Express. *Journal of Geophysical Research*, *114*, E00B44.

Gérard, J. C., Saglam, A., Piccioni, G., Drossart, P., Cox, C., Erard, S., ... Sánchez-Lavega, A. (2008). Distribution of the O_2 infrared nightglow observed with VIRTIS on board Venus Express. *Geophysical Research Letters*, *35*, L02207.

Gérard, J. C., Saglam, A., Piccioni, G., Drossart, P., Montmessin, F., & Bertaux, J. (2009). Atomic oxygen distribution in the Venus mesosphere from observations of O_2 infrared airglow by VIRTIS-Venus Express. *Icarus*, *199*, 264-272.

Gröller, H., Lammer, H., Lichtenegger, H. I. M., Pfleger, M., Dutuit, O., Shematovich, V. I., ... Biernat, H. K. (2012). Hot oxygen atoms in the venus nightside exosphere. *Geophysical Research Letters*, *39*, L03202,.

Gröller, H., Shematovich, V. I., Lichtenegger, H. I. M., Lammer, H., Pfleger, M., Kulikov, Y. N., ... Biernat, H. K. (2010). Venus' atomic hot oxygen environment. *Journal of Geophysical Research*, *115*, E12017.

Hinteregger, H. E., Fukui, K., & Gilson, G. R. (1981). Observational, reference and model data on solar euv from measurements on AE-E. *Geophysical Research Letters*, *8*, 1147-1150.

Hodges, R., & Tinsley, B. (1986). The influence of charge exchange on the velocity distribution of hydrogen in the Venus exosphere. *Journal of Geophysical Research*, *91*, 13649-13658.

Hodges, R. R. (2000). Distributions of hot oxygen for Venus and Mars. *Journal of Geophysical Research*, *105*(E3), 6971–6981.

Hueso, R., Sánchez-Lavega, A., Piccioni, G., Drossart, P., Gérard, J. C., Khatuntsev, I., ... Migliorini, A. (2008). Morphology and dynamics of Venus oxygen airglow from Venus Express/Visible and infrared Thermal Imaging Spectrometer observations. *Journal of Geophysical Research*, *113*, E12.

Kella, D., Vejby-Christensen, L., Johnson, P. J., Pedersen, H. B., & Andersen, L. H. (1997). The source of green light emission determined from a heavy-ion storage ring experiment. *Science*, *276*(5318), 1530-1533.

Kharchenko, V., Dalgarno, A., Zygelman, B., & Yee, J.-H. (2000). Energy transfer in collisions of in the terrestrial atmosphere oxygen atoms. *Journal of Geophysical Research*, *105*(A11), 24,899-24,906.

Knudsen, W. C., Spenner, K., Miller, K. L., & Novak, V. (1980). Transport of ionospheric O^+ ions across the Venus terminator and implications. *Journal of Geo-*

physical Research, *85*(A13), 7803-7810.

Lee, C., & Richardson, M. I. (2010). A general circulation model ensemble study of the atmospheric circulation of Venus. *Journal of Geophysical Research*, *115*(E04002).

Lee, Y., Combi, M. R., Tenishev, V., Bougher, S. W., Deighan, J., Schneider, N. M., ... Jakosky, B. M. (2015). A comparison of 3-d model predictions of Mars' oxygen corona with early MAVEN IUVS observations. *Geophysical Research Letters*, *42*, 9015–9022.

Lee, Y., Combi, M. R., Tenishev, V., Bougher, S. W., & Lillis, R. J. (2015). Hot oxygen corona at Mars and the photochemical escape of oxygen - improved description of the thermosphere, ionosphere and exosphere. *Journal of Geophysical Research (Planets)*, *120*.

Lee, Y., Dong, C., Pawlowski, D., Thiemann, E., Tenishev, V., Mahaffy, P., ... Eparvier, F. (2018). Effects of a solar flare on the Martian hot O corona and photochemical escape. *Geophysical Research Letters*, *45*(14), 6814-6822.

Lee, Y., Fang, X., Gacesa, M., Ma, Y., Tenishev, V., Mahaffy, P., ... Jakosky, B. (2020). Effects of global and regional dust storms on the martian hot o corona and photochemical loss. *Journal of Geophysical Research: Space Physics*, *125*(4), e27115.

Lellouch, E., Corvisier, J., Lim, T., Bockelée-Morvan, D., Leech, K., Hanner, M. S., ... Keller, H. U. (1998). Evidence for water ice and estimate of dust production rate in comet Hale-Bopp at 2.9 au from the Sun. *Astronomy and Astrophysics*, *339*(1), L9-L12.

Lichtenegger, H. I. M., Gröller, H., Lammer, H., Kulikov, Y. N., & Shematovich, V. I. (2009). On the elusive hot oxygen corona of venus. *Geophysical Research Letters*, *36*, L10204.

Lillis, R., Brain, D., Bougher, S., Leblanc, F., Luhmann, J., Jakosky, B., ... Lin, R. (2015, 357–422). Characterizing atmospheric escape from Mars today and through time, with MAVEN. *Space Science Reviews*, *195*.

Mehr, F. J., & Biondi, M. A. (1969). Electron temperature dependence of recombination of O_2^+ and N_2^+ ions with electrons. *Physical Review*, *181*, 1.

Nagy, A. F., Cravens, T. E., Yee, J.-H., & Stewart, A. I. F. (1981). Hot oxygen atoms in the upper atmosphere of Venus. *Geophysical Research Letters*, *8*, 629-632.

Parkinson, C. D., Bougher, S. W., Mills, F., Yung, Y. L., Brecht, A., Shields, D., & Liemohn, M. (2021). Modeling of observations of the OH nightglow in the venusian mesosphere. *Icarus*, *368*, 114580.

Pätzold, M., Häusler, B., Bird, M. K., Tellmann, S., Mattei, R., Asmar, S. W., ... Tyler, G. L. (2007). The structure of Venus' middle atmosphere and ionosphere. *Nature*, *450*(7170), 657–660.

Paxton, L. J., & Meier, R. R. (1986). Reanalysis of Pioneer Orbiter ultraviolet spectrometer data: OI 1304 intensities and atomic oxygen densities. *Geophysical Research Letters*, *13*(3), 229-232.

Piccialli, A., Tellmann, S., Titov, D., Limaye, S., Khatuntsev, I., Pätzold, M., & Häusl, B. (2012). Dynamical properties of the Venus mesosphere from the radio-occultationexperiment VeRa onboard Venus Express. *Icarus*.

Piccialli, A., Titov, D. V., Grassi, D., Khatuntsev, I., Drossart, P., Piccioni, G., & Migliorini, A. (2008). Cyclostrophic winds from the visible and infrared thermal imaging spectrometer temperature sounding: A preliminary analysis. *Journal of Geophysical Research (Planets)*, *113*, E00B11.

Piccioni, G., Zasova, L., Migliorini, A., Drossart, P., Shakun, A., ... Cardesin-Moinelo, A. (2009). Near-IR oxygen nightglow observed by VIRTIS in the Venus upper atmosphere. *Journal of Geophysical Research*, *114*, E00B38.

Roldán, C., López-Valverde, M., López-Puertas, M., & Edwards, D. (2000). Non-LTE infrared emissions of CO_2 in the atmosphere of Venus. *Icarus*, *147*(1), 11

- 25.

Schubert, G., Bougher, S. W., Covey, C. C., Genio, A. D. D., Grossman, A. S., Hollingsworth, J. L., ... Young, R. E. (2007). Exploring venus as a terrestrial planet. In L. W. Esposito, E. R. Stofan, & T. E. Cravens (Eds.), (p. 101-120). AGU Geophysical Monographs.

Soret, L., Gérard, J. C., Montmessin, F., Piccioni, G., Drossart, P., & Bertaux, J. L. (2012). Atomic oxygen on the venus nightside: Global distribution deduced from airglow mapping. *Icarus*, *217*, 849-855.

Soret, L., Gérard, J.-C., Piccioni, G., & Drossart, P. (2014). Time variations of $O_2(a^1\Delta)$ nightglow spots on the venus nightside and dynamics of the upper mesosphere. *Icarus*, *237*, 306 - 314.

Stewart, A. I. F., Gérard, J., Rusch, D. W., & Bougher, S. W. (1980). Morphology of the Venus ultraviolet night airglow. *Journal of Geophysical Research*, *80*.

Stiepen, A., Gérard, J.-C., Dumont, M., Cox, C., & Bertaux, J.-L. (2013). Venus nitric oxide nightglow mapping from SPICAV nadir observations. *Icarus*, *226*(1), 428 - 436.

Taylor, H. A., Brinton, H. C., Bauer, S. J., Hartle, R. E., Cloutier, P. A., & Daniell, R. E. (1980). Global observations of the composition and dynamics of the ionosphere of Venus: Implications for the solar wind interaction. *Journal of Geophysical Research*, *85*(A13), 7765-7777.

Tenishev, V., Rubin, M., Tucker, O. J., Combi, M. R., & Sarantos, M. (2013). Kinetic modeling of sodium in the lunar exosphere. *Icarus*, *226*(2), 1538–1549.

Tenishev, V., Shou, Y., Borovikov, D., Lee, Y., Fougere, N., Michael, A., & Combi, M. R. (2021). Application of the Monte Carlo method in modeling dusty gas, dust in plasma, and energetic ions in planetary, magnetospheric, and heliospheric environments. *Journal of Geophysical Research: Space Physics*, *126*, e2020JA028242. doi: https://doi.org/10.1029/2020JA028242

Valeille, A., Combi, M. R., Bougher, S. W., Tenishev, V., & Nagy, A. F. (2009). Three-dimensional study of Mars upper thermosphere/ionosphere and hot oxygen corona: 2. solar cycle, seasonal variations, and evolution over history. *Journal of Geophysical Research*, *114*, E11006.

Valeille, A., Combi, M. R., Tenishev, V., Bougher, S. W., & Nagy, A. F. (2010). A study of suprathermal oxygen atoms in Mars upper thermosphere and exosphere over the range of limiting conditions. *Icarus*, *206*(1), 18-27.

Valeille, A., Tenishev, V., Bougher, S. W., Combi, M. R., & Nagy, A. F. (2009). Three-dimensional study of Mars upper thermosphere/ionosphere and hot oxygen corona: 1. general description and results at equinox for solar low conditions. *Journal of Geophysical Research*, *114*, E11005.

von Zahn, U., Fricke, K. H., Hoffmann, H., & Pelka, K. (1979). Venus: eddy coefficients in the thermosphere and the inferred helium content of the lower atmosphere. *Geophysical Research Letters*, *6*(5).

Zalucha, A. M., Brecht, A. S., Rafkin, S., Bougher, S. W., & Alexander, M. J. (2013). Incorporation of a gravity wave momentum deposition parameterization into the Venus Thermosphere General Circulation Model (VTGCM). *Geophysical Research Letters*, *118*, 147-160.